Kinetic Mechanism of Metallo-β-lactamase L1 from *Stenotrophomonas maltophilia*[†]

Silvia McManus-Munoz and Michael W. Crowder*

Department of Chemistry and Biochemistry, Miami University, 112 Hughes Hall, Oxford, Ohio 45056

Received November 6, 1998; Revised Manuscript Received December 8, 1998

ABSTRACT: The reaction of nitrocefin with metallo-β-lactamase L1 from *Stenotrophomonas maltophilia* was studied using rapid-scan and stopped-flow ultraviolet−visible (UV−vis) studies in an effort to discern the kinetic mechanism used by L1 to hydrolyze penicillins and cephalosporins. Rapid-scan and stopped-flow UV−vis studies of nitrocefin hydrolysis by L1 identified three species: (1) the substrate (nitrocefin) displayed an absorbance peak at 390 nm ($\epsilon = 11\,500\ M^{-1}\ cm^{-1}$) that decreased during the reaction with a rate constant of $170 \pm 30\ s^{-1}$; (2) the product (hydrolyzed nitrocefin) displayed an absorbance peak at 485 nm ($\epsilon = 17\,420\ M^{-1}\ cm^{-1}$) that increased during the reaction with rate constant of $40 \pm 1\ s^{-1}$; and (3) an intermediate displayed an absorbance peak at 665 nm ($\epsilon = 32\,000\ M^{-1}\ cm^{-1}$) that increased initially with a rate constant of $190 \pm 3\ s^{-1}$ and then decreased with a rate constant of $38 \pm 2\ s^{-1}$. Single-turnover experiments demonstrated that there were no pre-steady-state bursts in the reaction of L1 with nitrocefin; moreover, the progress curves could be fit to a kinetic mechanism that includes the formation of a transient intermediate by using KINSIM and the rate constants given above. Progress curves from experiments conducted at different reaction conditions or with a different substrate could also be fit to the proposed kinetic mechanism. The evidence for the presence of an intermediate along with kinetic simulations supports a hydrolytic mechanism for L1 that involves an intermediate whose breakdown is rate-determining.

β-Lactamases are bacterial enzymes that catalyze the hydrolysis of β-lactam antibiotics, rendering the antibiotics ineffective as inhibitors of bacterial cell wall synthetic enzymes (*1*). These enzymes have been classified by several groups, based on requirement of Zn(II), on substrate specificity, and on interactions with inhibitors (*2*−*7*). Groups 1, 2, and 4 β-lactamases are the most prevalent of these enzymes and utilize an active-site serine for the nucleophilic attack on the β-lactam carbonyl (*1*). Fortunately, there are clinically useful inhibitors for many of the bacterial strains that harbor one of these β-lactamases (*7*). The group 3 β-lactamases are distinct in that they require Zn(II) for activity and that there are no clinically useful inhibitors for these enzymes (*8*). The group 3 β-lactamases have been further classified on the basis of their substrate specificity; the group 3a enzymes, which are represented by the β-lactamases from *Bacillus cereus*, *Bacteroides fragilis*, and *Stenotrophomonas maltophilia*, prefer cephalosporins and penicillins as substrates and contain 2 Zn(II) ions per monomer. The Group 3b enzyme, which is represented by the β-lactamase from *Aeromonas hydrophila*, significantly hydrolyzes only carbapenems and requires only 1 Zn(II) for full catalytic activity (*9*). Rossolini et al. (*10*) have recently reported that metallo-β-lactamase from *Chrysiobacterium meningosepticum* may represent yet another molecular class of group 3 β-lactamases. The group 3a enzymes are further distinguishable on the basis of their metal binding ligands (*11*−*13*), Zn(II) binding affinity (*12*, *14*−*16*), interaction with mercaptan inhibitors (*17*, *18*), and subunit stoichiometries (*11*−*13*, *15*, *19*−*22*).

S. maltophilia is an increasingly important pathogen in nosocomial infections of immunocompromised patients suffering from cancer, cystic fibrosis, drug addiction, and AIDS and in patients with organ transplants and on dialysis (*23*−*30*). *S. maltophilia* strains that are resistant to penicillins, cephalosporins, and carbapenems have been isolated from clinical samples (*20*, *31*). *S. maltophilia* is inherently resistant to multiple antimicrobial agents due to its low outer membrane permeability (*32*) and is β-lactam-resistant due to its production of chromosomally expressed group 2e β-lactamase (L2) and group 3a β-lactamase (L1)[1] (*22*, *33*). The production of inhibitors to combat the latter enzymes is therefore needed urgently. To prepare mechanistically relevant inhibitors, information is needed about the kinetic mechanism so that the slowest steps of the mechanism catalyzed by L1 can be targeted for the preparation of inhibitors. This work describes rapid-scan/stopped-flow kinetic studies of L1 and its reaction with nitrocefin. A kinetic mechanism is offered that accounts for all detected species generated during catalytic turnover and is supported by kinetic simulations of data collected at single-turnover and at differing reaction conditions.

EXPERIMENTAL PROCEDURES

General. Metallo-β-lactamase L1 was purified as described previously (*15*). Protein purity was ascertained by SDS−PAGE, and the metal content of each enzyme preparation

[†] The authors acknowledge NIH R29 AI40052 (to M.W.C.) for funding this work.

* Corresponding author: Phone (513) 529-7274; FAX (513) 529-5715; e-mail crowdemw@muohio.edu.

[1] Abbreviations: BSA, bovine serum albumin; CcrA, metallo-β-lactamase from *Bacteroides fragilis*; E•I, intermediate; ϵ, extinction coefficient; k_{cat}, turnover number; K_d, dissociation constant; K_m, Michaelis constant; L1, metallo-β-lactamase from *Stenotrophomonas maltophilia*; P, product; SDS, sodium dodecyl sulfate; S, substrate; UV−vis, ultraviolet−visible.

10.1021/bi9826512 CCC: $18.00 © 1999 American Chemical Society
Published on Web 01/12/1999

was determined with a Perkin-Elmer inductively coupled plasma emission spectrometer. Steady-state kinetic parameters, K_m and k_{cat}, were determined for each protein preparation prior to rapid kinetic studies. The buffer used in all studies was 50 mM cacodylate, pH 7.0. Nitrocefin stock solutions were made by dissolving nitrocefin (Becton Dickinson) in 50 mM cacodylate, pH 7.0, followed by filtering the solution through a 0.45 μm syringe filter.

Stopped-Flow UV−Vis Studies. Stopped-flow UV−vis studies were conducted on a Photal RA-401 (Otsuka Electronics) UV−vis spectrophotometer equipped with a 1 cm path length and thermostated to 25 °C. The data were recorded on an IBM AT personal computer and converted to Ascii files using QuickBasic.

In stopped-flow studies, a minimum of three reproducible experiments were conducted and averaged. Hydrolyzed nitrocefin formation was monitored at 485 nm, and the absorbance data were converted to concentration data by using a molar extinction coefficient of 17 420 M^{-1} cm^{-1}. Nitrocefin depletion was monitored at 390 nm, and the absorbance data were converted to concentration data by using a molar extinction coefficient of 11 500 M^{-1} cm^{-1}. The molar extinction coefficients of nitrocefin and hydrolyzed nitrocefin were determined by using known standards of substrate or product and Beer's law. The product and substrate absorbance data were corrected for the absorbance of nitrocefin or hydrolyzed nitrocefin at 485 and 390 nm, respectively. In addition, each set of data was corrected for the instrument dead time (2.5 ms). Each set of concentration of product versus time profiles were fit to $y = y_0 + a(1 - e^{-k_3x})$, and the concentration of substrate versus time profiles were fit to $y = y_0 + ae^{-k_2x}$ with Sigmaplot 4.01, where y is the concentration of product and substrate, respectively, and x is the time in seconds.

The formation and decay of intermediate with nitrocefin as the substrate were monitored at 665 nm. The molar extinction coefficient of intermediate was estimated by collecting data from several stopped-flow experiments while varying L1 and nitrocefin concentrations and using Beer's law. The concentration of intermediate was calculated from the formula $[\text{intermediate}] = [S]_{initial} - ([S]_t + [P]_t)$, where $[S]_{initial}$ is the initial substrate concentration in the reaction, $[S]_t$ is the substrate concentration at time t, and $[P]_t$ is the product concentration at time t. The calculated molar extinction coefficient at 665 nm for the intermediate of nitrocefin hydrolysis is 32 000 ± 2000 M^{-1} cm^{-1}. The absorbance data for the intermediate was corrected for the instrument dead time (2.5 ms). Each set of concentration of absorbing species at 665 nm versus time plots were fit to a double-exponential equation with floating end point, $y = ae^{-k_2x} + be^{-k_3x} + e$, where y is the concentration of intermediate and x is the time in seconds.

When BRL42715 was used as the substrate, the formation of product was monitored at 358 nm. The absorbance data was converted to concentration data by using a molar extinction coefficient of 1140 M^{-1} cm^{-1} (*34*).

Rapid Scans of L1 Hydrolysis. Rapid-scan UV−vis spectra of L1 hydrolysis reactions were collected on a Photal RA-401 (Otsuka Electronics) UV−vis spectrophotometer equipped with a 1 cm path length and thermostated to 25 °C. The data were recorded on an IBM AT personal computer and converted to Ascii files by using QuickBasic. A spectral range of 190 nm is the largest window allowed by this instrument. In a typical experiment, 16 scans over a 190 nm range were collected at different time points. The length of time for the scan was determined by the gate time, which was normally ca. 10 ms, and the time between each scan was set by the time interval, i.e., a time interval of 1 with a gate time of 10 ms indicates that a scan was taken over a period of 10 ms, one pause of 10 ms, followed by another 10 ms scan. Three sets of 16 scans were taken for each experiment and averaged.

Fluorescence Titrations. Fluorescence titrations were performed at 25 °C in 50 mM cacodylate, pH 7.0, on a Perkin-Elmer LS50 fluorometer. Hydrolyzed nitrocefin was prepared by allowing a 25 mM sample of nitrocefin in 50 mM cacodylate buffer, pH 7.0, containing 50 nM L1 to incubate for 5 h at 37 °C. The reaction was followed by UV−vis. L1 was removed from the mixture by using a Centricon-10 ultrafiltrator, and the resulting solution of hydrolyzed nitrocefin was used as a titrant. The thermodynamic dissociation constant (K_d) of hydrolyzed nitrocefin binding to L1 was evaluated by following the quenching of intrinsic L1 tryptophan fluorescence at 340 nm upon excitation at 280 nm as a function of added hydrolyzed nitrocefin (*35*, *36*). The observed fluorescence readings were corrected for inner filter effects by the simultaneous titration of a tryptophan standard solution and for the denaturation of L1 during the titration, which was less than 10%. The concentration of L1 in the titrations was 500 nM. Following corrections for L1 denaturation, sample dilution upon addition of titrant, and inner filter effects, the corrected data were fit to a quadratic equation using CurveFit version 0.8, as previously reported (*35*−*37*).

Kinetic Simulations. The kinetic mechanism for L1 hydrolysis, according to Scheme 1, was simulated by using the program KINSIM (*37*−*41*). The values for flux and integral tolerances were left as the default values of 0.02 and 1×10^{-6}, respectively. Errors in rate constants predicted by KINSIM were evaluated by using FITSIM (*38*, *39*). A Marquardt regression algorithm was used to fit the KINSIM-generated profile to the data sets.

The data were also simulated by using Excel as described by Bruist (*42*). The equations used to generate simulated change in concentration (i.e., ΔE) versus change in time (Δt) profiles were as follows:

$$\Delta E = (-k_1[E][S] + k_{-1}[E\cdot S] + k_4[E\cdot P] - k_{-4}[E][P])\Delta t$$

$$\Delta S = (-k_1[E][S] + k_{-1}[E\cdot S])\Delta t$$

$$\Delta E\cdot S = (k_1[E][S] - [E\cdot S](k_{-1} + k_2) + k_{-2}[E\cdot I])\Delta t$$

$$\Delta E\cdot I = (k_2[E\cdot S] - [E\cdot I](k_{-2} + k_3) + k_{-3}[E\cdot P])\Delta t$$

$$\Delta E\cdot P = (k_3[E\cdot I] - [E\cdot P](k_{-2} + k_4) + k_{-4}[E][P])\Delta t$$

$$\Delta P = (k_4[E\cdot P] - k_{-4}[E][P])\Delta t$$

RESULTS

Rapid Scan UV−Vis Studies of Nitrocefin Hydrolysis by L1. To study the kinetic mechanism of L1, the colormetric cephalosporin nitrocefin was used as the substrate (*43*). The reaction of 76 μM L1 with 88 μM nitrocefin was monitored

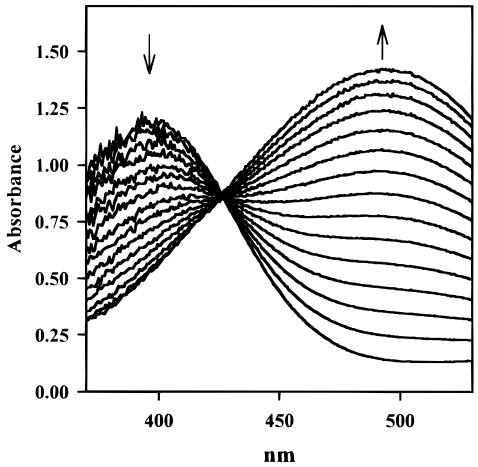

FIGURE 1: Rapid-scan UV−vis spectra of the reaction of 76 μM L1 with 88 μM nitrocefin in 50 mM cacodylate, pH 7.0, at 25 °C. The spectra were collected with the following experimental parameters: center, 450 nm; scan range, 355−545 nm; gate time, 10 ms; time interval, 1; number of spectra, 16.

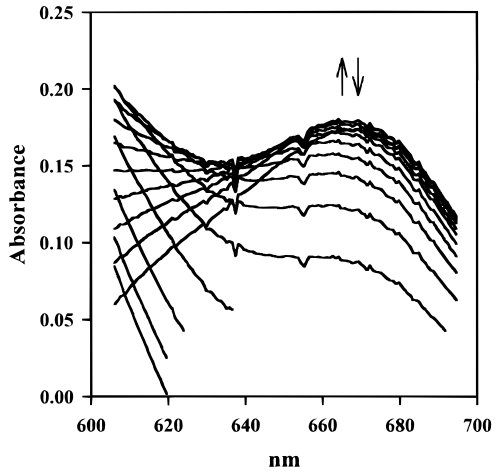

FIGURE 2: Rapid-scan UV−vis spectra of the reaction of 76 μM L1 with 88 μM nitrocefin in 50 mM cacodylate, pH 7.0, at 25 °C. The spectra were collected with the following experimental parameters: center, 650 nm; scan range, 605−695 nm; gate time, 10 ms; time interval, 1; number of spectra, 16.

over a 500 ms time period between 355 and 545 nm (Figure 1). The only features observed are a broad absorption band with a maximum at 390 nm that decreases over time and a broad band with a maximum at 485 nm that emerges over time. UV−vis spectroscopic studies reveal that nitrocefin has an absorbance maximum at 390 nm ($\epsilon = 11\,500$ M^{-1} cm^{-1}), while hydrolyzed nitrocefin has an absorbance maximum at 485 nm ($\epsilon = 17\,420$ M^{-1} cm^{-1}) (data not shown) (*43*).

The spectral range was extended to 600−700 nm to probe whether any other absorbing species were being produced in the reaction of 76 μM L1 and 88 μM nitrocefin during the 500 ms time period. A peak at 665 nm ($\epsilon = 32\,000$ M^{-1} cm^{-1}) emerged in the first 50 ms of the reaction and decayed over the subsequent 400 ms (Figure 2).

Stopped-Flow UV−Vis Studies of Nitrocefin Hydrolysis by L1. To further probe the reaction of L1 with nitrocefin, stopped-flow kinetic studies were conducted under single-turnover conditions (Figure 3A). Product formation (hydrolyzed nitrocefin, ●) and substrate depletion (nitrocefin, ◆) were monitored at 485 and 390 nm, respectively, over a 200 ms time period. The initial concentrations of L1 and

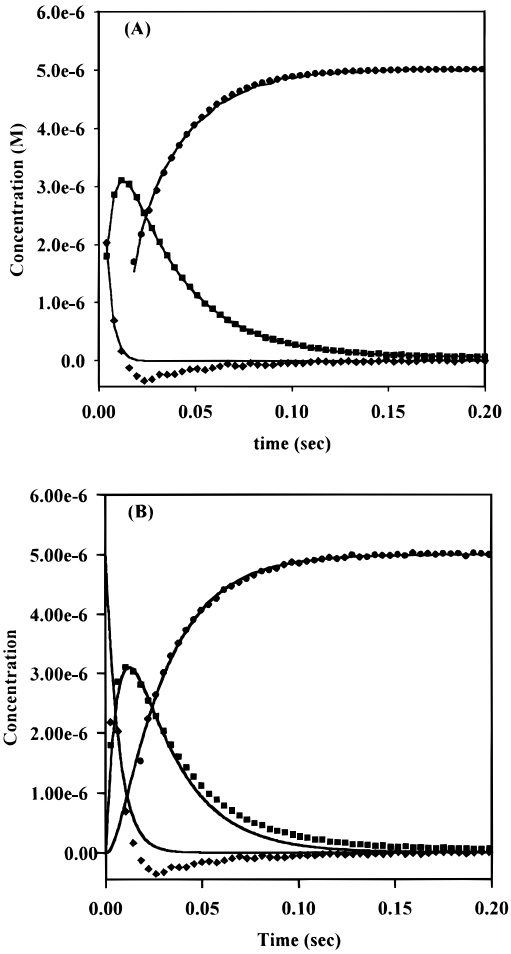

FIGURE 3: (A) Stopped-flow UV−vis studies of 25 μM L1 and 5 μM nitrocefin in 50 mM cacodylate, pH 7.0, at 25 °C. The data points for product (●), substrate (◆), and intermediate (■) were converted from stopped-flow absorbance data to concentration data as described in Experimental Procedures. The lines through the three sets of data represent the fit of the data to an exponential equation, as described in Experimental Procedures. (B) Concentration versus time plots of the reaction of 25 μM L1 with 5 μM nitrocefin monitoring product formation (●), substrate depletion (◆), and the fate of the intermediate (■) in 50 mM cacodylate, pH 7.0, at 25 °C. The absorbance data taken from stopped-flow UV−vis traces were converted into concentration data as described in Experimental Procedures. The curves on the plot were calculated by using KINSIM with the rate constants summarized in Table 1. The KINSIM-generated lines were calculated as ([P] + [E·P]) (line through ●), ([S] + [E·S]) (line through ◆), and [E·I] (line through ■) versus time plots.

nitrocefin were 25 and 5 μM, respectively. The progress curve when product formation was monitored showed a linear increase in absorbance until substrate was depleted. Fitting these data to an exponential equation resulted in a rate constant of 40 ± 1 s^{-1} for product formation. The substrate progress curve exhibited a linear decrease in absorbance until substrate was depleted. Fitting these data to an exponential equation resulted in a rate constant of 170 ± 30 s^{-1} for substrate depletion. The large relative error of the latter rate constant is due to the small number of data points collected over the first 10−20 ms and to the poor fitting of the data during the 20−60 ms time period when there is a dip in the data. This dip is present in all stopped-flow studies conducted; however, the size of the dip and its duration greatly varies. We therefore attribute it to a spectrophotometer

artifact. There were no detectable burst phases in these progress curves. To test whether these experiments were actually at single-turnover conditions, stopped-flow studies with 100 μM L1 and 5 μM nitrocefin were conducted. These experiments yielded concentration versus time profiles that were superimposable on those in Figure 3A (data not shown).

The reaction of nitrocefin and L1 was also conducted under single-turnover conditions monitoring the reaction at 665 nm (Figure 3A, ■). The progress curve for this experiment exhibits a rapid increase in absorbance at 665 nm over the first 25 ms, followed by a decay of the absorbing species over the next 100 ms. Fitting these data to a double-exponential equation resulted in rate constants of 190 ± 3 and 38 ± 2 s^{-1} for the formation and decay of the species absorbing at 665 nm, respectively.

Scheme 1

$$E + S \underset{k_{-1}}{\overset{k_1}{\rightleftharpoons}} E\cdot S \underset{k_{-2}}{\overset{k_2}{\rightleftharpoons}} E\cdot I \underset{k_{-3}}{\overset{k_3}{\rightleftharpoons}} E\cdot P \underset{k_{-4}}{\overset{k_4}{\rightleftharpoons}} E + P$$

KINSIM Simulations of the Single-Turnover Experiments. To propose and test a kinetic mechanism for L1 and its reaction with nitrocefin, the kinetic simulation program KINSIM was used (*39*). One mechanism that accounts for all of the species involved in the reaction is given in Scheme 1. The two binding steps, given by the rate constants k_1 and k_{-4}, were set to diffusion-controlled limits of 10^8 M^{-1} s^{-1}. The rate constant k_4 was calculated from the expression $K_d = k_{off}/k_{on}$, where K_d is the dissociation constant for E·P, k_{off} is k_4, and k_{on} is k_{-4} (*44*). Fluorescence titrations of L1 with hydrolyzed nitrocefin were used to calculate a lower limit for the K_d of product binding to E·P (350 μM) (data not shown). This value is a lower limit because the solubility limits of product prevented our ability to completely saturate L1 with product. Product inhibition studies of nitrocefin hydrolysis by L1 confirmed that hydrolyzed nitrocefin binds very weakly to L1 and does not appreciably inhibit L1 even at concentrations up to 500 μM (data not shown). The rate constants k_{-2} and k_{-3} were set to very small values because the hydrolysis of nitrocefin is essentially irreversible, and attempts to monitor substrate production when L1 is incubated with product were unsuccessful. Kinetic simulations demonstrated that the shape of simulated concentration versus time plots is essentially independent of k_1, k_4, and k_{-4} even if these constants were varied over several orders of magnitude. However, the shapes of the curves were highly dependent on the values of k_{-1}, k_2, and k_3. The values of k_2 and k_3 were set to the experimentally determined values of 190 and 40 s^{-1}, respectively. In Figure 3B the concentration versus time data points taken from the single-turnover experiments and the simulated lines ([S + E·S], [E·I], and [P + E·P] versus time) calculated by KINSIM are shown, using the rate constants in Table 1 and the kinetic mechanism in Scheme 1. FITSIM was used to evaluate uncertainties in fitting of the data, and these results are shown in Table 2. Similar simulated profiles and rate constants were obtained by using Excel to fit the data (not shown).

To further test the kinetic mechanism given in Scheme 1 and the rate constants in Table 1, stopped-flow studies under different reaction conditions were conducted, and the data were fit to the proposed mechanism by using KINSIM. In experiments where the concentration of L1 is varied over 4 orders of magnitude and the concentration of nitrocefin is fixed at 5.0 μM, the KINSIM-predicted concentration ([E·P + P]) versus time profiles qualitatively fit the experimental data (Figure 4). Similar results are observed when substrate depletion or intermediate formation and decay were monitored in the presence of varied concentrations of L1.

Table 1: Kinetic Rate Constants Used in Simulations in Figures 3B and 4

rate constant	value used in simulation
k_1	10^8 M^{-1} s^{-1}
k_{-1}	550 s^{-1}
k_2	190 s^{-1}
k_3	40 s^{-1}
k_4	3.5×10^4 s^{-1}
k_{-4}	10^8 M^{-1} s^{-1}

Table 2: Errors in Rate Constants

rate constant	fit to exponential equation	fit with FITSIM
k_{-1}	not determined	550 ± 90 s^{-1}
k_2	190 ± 20 s^{-1}	198 ± 6 s^{-1}
k_3	40 ± 1 s^{-1}	39 ± 1 s^{-1}

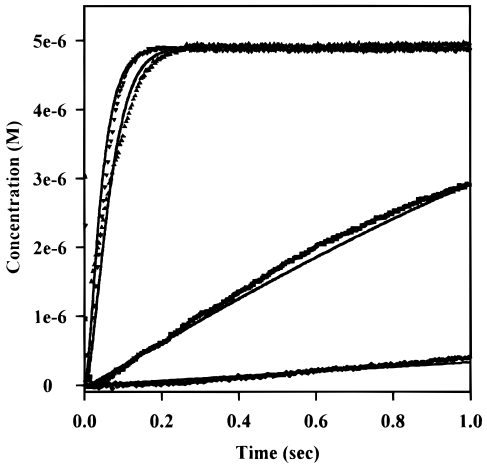

FIGURE 4: Concentration versus time plots of the reaction of 5 μM nitrocefin with 25 μM (▼), 5 μM (▲), 0.20 μM (■), and 0.020 μM (●) concentration of L1 in 50 mM cacodylate, pH 7.0, at 25 °C. The absorbance data taken from stopped-flow UV−vis traces were converted into concentration data as described in Experimental Procedures. The curves on the plot were calculated by using KINSIM with the rate constants summarized in Table 1. The KINSIM-generated lines were calculated as ([P] + [E·P]) versus time plots.

Use of BRL 42715 as the Substrate. To determine if the mechanism in Scheme 1 could also account for the reaction of L1 with an alternative substrate, rapid kinetic studies were conducted with BRL42715 as the substrate (*34*). Rapid-scan UV−vis spectra over 240−550 nm were collected for a reaction containing 55 μM L1 and 288 μM BRL42715. The resulting spectra revealed two features: a peak at 303 nm that decreased over time and a peak at 358 nm that increased over time (data not shown). The former feature represents unhydrolyzed BRL42715 (substrate), while the latter feature is the absorption maximum of hydrolyzed BRL42715 (product) (*34, 45*). There were no other features in the spectra.

Stopped-flow studies were conducted with 109 μM L1 and 117 μM BRL42715 (Figure 5, ●). The resulting product concentration versus time progress curves were similar in

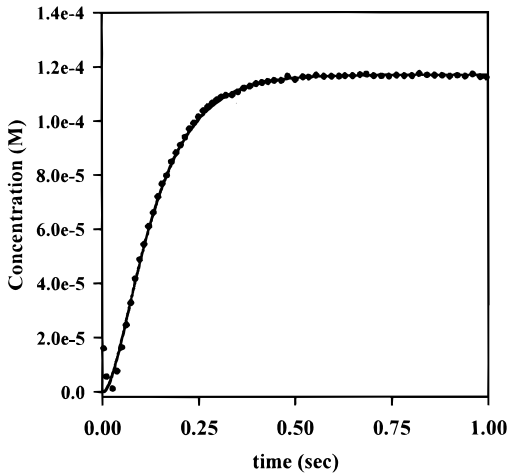

FIGURE 5: Concentration versus time plot of the reaction of 109 μM L1 with 117 μM BRL42715 monitoring the formation of hydrolyzed BRL42715 (●) in 50 mM cacodylate, pH 7.0, at 25 °C. The absorbance data taken from stopped-flow UV−vis traces were converted into concentration data as described in Experimental Procedures. The curves on the plot were calculated by using KINSIM with the rate constants described in the text. The KINSIM-generated lines were calculated as ([P] + [E·P]) versus time plots.

appearance to those observed in the nitrocefin experiments when product formation was followed. Using the kinetic mechanism in Scheme 1, KINSIM was used to simulate the reaction profile (line in Figure 5). The kinetic rate constants used for the simulated line are $k_1 = 10^8$ M^{-1} s^{-1}, $k_{-1} = 2.4 \times 10^4$ s^{-1}, $k_2 = 49 \pm 18$ s^{-1}, $k_3 = 20 \pm 9$ s^{-1}, $k_4 = 3.5 \times 10^4$ s^{-1}, and $k_{-4} = 10^8$ M^{-1} s^{-1}. Attempts to fit the substrate depletion were unsuccessful due to weak absorption of substrate and the resulting noisy data.

DISCUSSION

Previous biochemical and sequence data have suggested structural and mechanistic heterogeneity among the metallo-β-lactamases, even among the class 3a enzymes. For example, the metallo-β-lactamases from *S. maltophilia* (L1) and *B. fragilis* (CcrA) contain two tightly bound Zn(II) ions per monomer and require both Zn(II)s for full catalytic activity (*13*−*15*), while metallo-β-lactamase II from *B. cereus* contains one tightly bound Zn(II) and a more loosely bound Zn(II) (*12, 16, 46*). The β-lactamase from *A. hydrophila* requires only one Zn(II); in fact, the binding of a second Zn(II) is inhibitory (*9*). The crystal structures of L1, CcrA, and β-lactamase II reveal distinct structural aspects of the enzymes with CcrA and β-lactamase II being more similar (*11, 13, 46*−*48*). L1 does not utilize the same amino acid ligands to bind Zn(II), and residues predicted to be important for catalysis for CcrA are either not sequence- (Lys at position 171) or position-conserved (Asn at position 180) (*11, 13*). pH dependence studies over the pH range of 4−10.5 on β-lactamase II indicated three catalytically important proton transfers (*49*), while similar studies on CcrA and L1 do not indicate similar findings (S. M. McManus and M. W. Crowder, unpublished results) (*21*). These differences among the metallo-β-lactamases is alarming because it suggests that one inhibitor might not be effective against all enzymes. This suggestion has been further supported by the different effacacies of a set of mercaptan-containing inhibitors on metallo-β-lactamases from several sources (*17, 18*). One way to overcome this potential problem is to characterize metallo-β-lactamases from a number of sources and exploit structural or mechanistic similarities for the generation of an inhibitor. The work presented here describes the kinetics characterization of metallo-β-lactamase L1 from *S. maltophilia*.

Nitrocefin, (6*R*)-3-(2,4-dinitrostyryl)-8-oxo-7-[(2-thienylacetyl)amino-5-thia-1-azabicyclo [4.2.0]oct-2-ene-2-carboxylic acid, was chosen as the substrate because the distinctive coloration of the hydrolyzed and unhydrolyzed species allowed for monitoring of each separately (Figure 1) (for the structure of nitrocefin see ref *43*). Over the spectral window of 355−545 nm, the substrate is apparently converted continuously over to product with the presence of one isosbestic point at 440 nm. However, the expanding of the spectral window out to 700 nm allowed for the detection of a species that formed in the first 50 ms of the reaction and decayed over the next 400 ms, when the experiment was conducted as described in the Figure 2 caption. This species absorbs quite strongly, with a calculated ϵ_{665nm} of 32 000 M^{-1} cm^{-1}. This is first evidence of an intermediate forming in the hydrolysis mechanism catalyzed by L1. The concentration and lifetime of this intermediate was dependent on [E] and [S]; therefore, the species that absorbs at 665 nm originates from E·S and has been abbreviated as E·I in Scheme 1. The denotation of E·I to describe a reaction intermediate does not imply a covalently bound species. A similar species is formed in the reaction of CcrA with nitrocefin (*21*).

To further probe the reaction of L1 and nitrocefin, stopped-flow kinetic studies were performed under single-turnover conditions (25 μM L1 and 5 μM nitrocefin), monitoring the reaction at 390 nm (substrate depletion, ◆), 485 nm (product formation, ●), and 665 nm (fate of the intermediate, ■) (Figure 3A). Single-turnover conditions ensure that all of the substrate is bound; therefore, the measured rate should be equal to the rate of the rate-limiting step(s) of the reaction (*44*). Therefore, each progress curve was fit to exponential equations, and substrate (and/or E·S) depletion occurred at 170 ± 30 s^{-1}, E·I formation occurred at 190 ± 3 s^{-1}, E·I breakdown occurred at 38 ± 2 s^{-1}, and E·P (and/or P) formation occurred at 40 ± 1 s^{-1}.

To propose a kinetic mechanism for L1, the simulation and fitting programs KINSIM and FITSIM were used (*39*). Before use of KINSIM, several assumptions were made: (1) E·S and S both absorb at 390 nm and have the same ϵ; (2) E·P and P both absorb at 485 nm and have the same ϵ, (3) k_{-2} and k_{-3} have very small values, essentially making the second and third steps irreversible; and (4) S and P bind to L1 at diffusion-controlled rates (10^8 M^{-1} s^{-1}). k_2 was set to 190 s^{-1}; this value was chosen over k_2 derived from substrate depletion data because of the better fit of E·I data to the exponential equation and the resulting lower error associated with this rate constant. k_3 was set to 40 s^{-1}, which is the rate constant derived from fitting product formation versus time data to an exponential equation. The mechanism chosen to fit the data was the simplest mechanism possible that accounted for the presence of an intermediate and for reversible binding of substrate and product (Scheme 1). A similar kinetic mechanism has been proposed for CcrA and its reaction with nitrocefin (*21*). [E + E·S], [E·P + P], and [E·I] versus time plots were generated by KINSIM with the

rate constants in Table 1 (Figure 3B), and FITSIM was used to estimate error in k_{-1}, k_2, and k_3 (Table 2). The simulations that best fit the single-turnover data were generated with k_{-1}, k_2, and k_3 values of 550 ± 90, 198 ± 6, and 39 ± 1 s^{-1}, respectively, indicating that the breakdown of E·I is rate-limiting.

Since the decay of E·I is rate-limiting, L1 apparently uses a kinetic mechanism (*44*), where $K_m = (k_{-1}k_3)/k_1k_2 = 1.1$ μM, $k_{cat} = k_2k_3/(k_2 + k_3) = 33$ s^{-1}, and $K_s = K_m[(k_2 + k_3)/k_3] = 6.5$ μM. The K_m and k_{cat} values for recombinant L1 hydrolysis of nitrocefin, determined by steady-state kinetic studies, are 4 ± 1 μM and 38 ± 1 s^{-1} (*15*), respectively. An explanation for the differences in K_m and k_{cat} determined from steady-state kinetics and from the simulated rate constants is that L1 might behave differently at micromolar concentrations (used in stopped-flow studies) than at nanomolar concentrations (used in steady-state kinetic experiments). Previous biochemical studies have indicated that L1 exists as a tetramer in solutions when the concentration of L1 is in the micromolar range (*11, 15*), but we are uncertain as to the aggregation state of L1 at nanomolar concentrations. If L1 is monomeric at nanomolar concentrations, we postulated that this form of the enzyme would not necessarily have the same activity as tetrameric L1.

To address whether possible aggregation of L1 in the stopped-flow experiments could explain the lower k_{cat} values, we varied the concentration of L1 over 4 orders of magnitude and evaluated whether k_3 changed at the different concentrations of L1. Figure 4 shows that k_3 does not change over this range of L1 concentrations. This result is consistent with stopped-flow studies in the presence of 0.5 mg/mL bovine serum albumin (BSA), which resulted in progress curves that were identical to reactions in the absence of BSA. L1 apparently exists as a tetramer at all of the concentrations tested, and BSA does not prevent the aggregation. A recent crystal structure of L1 revealed that the tetramerization of L1 is due to several hydrophobic contacts (*11*). We are currently generating site-directed mutations of the residues involved in these contacts to reduce or eliminate the tetramerization of L1, and kinetic studies on the resulting mutant enzymes should shed light on the issue of aggregation state/activity.

To ensure that we were using KINSIM properly and that the newer version of KINSIM (*39*) was generating the correct concentration versus time profiles, we also simulated progress curves by directly solving the differential equations of the kinetic mechanism in Scheme 1 by using Excel as described by Bruist (*42*). Using this method, we were able to predict the same rate constants for L1 and its reaction with nitrocefin under single-turnover conditions. Unfortunately, we have been unable to use commercially available curve-fitting programs to estimate errors in the calculated versus the experimental concentrations versus time plots due to the complexity of the differential equations.

To test the mechanism given in Scheme 1 and the rate constants in Table 1, stopped-flow studies were conducted under different reaction conditions. As shown in Figure 4, when the concentration of L1 is varied over 4 orders of magnitude, resulting experimental progress curves (data points in Figure 4) can be simulated by KINSIM with the rate constants in Table 1. Similar experiments monitoring substrate depletion or intermediate formation and decay could also be simulated by using KINSIM and the mechanism in Scheme 1.

To further test the mechanism, an alternative substrate, [(5*R*)-(2)-6-(1-methyl-1,2,3-triazol-4-ylmethylene)penem-3-carboxylic acid], BRL42715, was used in stopped-flow kinetic studies (for the structure of BRL42715, see ref 34). This compound was chosen because hydrolyzed and unhydrolyzed BRL42715 absorb in the visible region, and we had hoped that any detectable intermediate would also absorb in the visible region. However, rapid-scan UV−vis studies revealed only the presence of substrate and product in the wavelength region tested. Stopped-flow UV−vis studies monitoring the reaction at 358 nm yielded a concentration versus time plot that was similar in appearance to the nitrocefin product versus time plot and that could be simulated by using the mechanism in Scheme 1 by KINSIM (Figure 5, ●). The KINSIM progress curve (line in Figure 5) was generated by using different values for the rate constants k_{-1} [K_m for BRL42715 is 240 μM (*15*)], k_2, and k_3. With this substrate, the best fit of the experimental data was observed when k_3 is rate-limiting. Recently, Wang and Benkovic (*21*) have reported that the rate-limiting step for CcrA-catalyzed hydrolysis of nitrocefin is breakdown of E·I, where k_2 is at least 10 times greater than k_3. In the case of L1, the rate-limiting step of the hydrolysis reaction is also the breakdown of E·I; however, the difference in values of k_2 and k_3 may be dictated by the substrate.

The identity of E·I is currently unknown; however, the detection of E·I in UV−vis studies at 665 nm may offer some clues as to its structure. The red shift of E·I's absorbance maximum to 665 nm suggests that E·I has a lower energy than either nitrocefin or hydrolyzed nitrocefin. One scenario that could explain such an energy difference is increased conjugation in E·I as compared to S, E·S, or E·P. Wang et al. (*50*) have recently proposed a negatively charged nitrogen in the six-membered ring of hydrolyzed nitrocefin intermediate; such a species would extend the conjugation of the 2,4-dinitrostyryl substituent of nitrocefin into the six-membered ring and would be expected to result in a lower energy species. The excess negative charge on the nitrogen could be stabilized by Zn(2) [the second Zn(II) site with His89, His225, Asp88, a terminal water, and a bridging water as ligands] of L1, which has been postulated to interact with the substrate ring nitrogen, and possibly by Tyr191 via a hydrogen bond (*11*). The generation of Y191 mutants is currently in progress.

Previously, cryoenzymological and rapid kinetic studies on the metallo-β-lactamase II from *B. cereus* were used to propose a branched kinetic pathway for the enzyme-catalyzed hydrolysis of penicillin G and nitrocefin (*51, 52*). UV−vis spectroscopic studies on the Co(II)-substituted form of the enzyme allowed for the detection of all of the intermediates formed in the proposed pathway.

In contrast, the results of stopped-flow and rapid-scan UV−vis studies with the metallo-β-lactamases L1 and CcrA (*21, 50*) reveal reaction profiles that do not have pre-steady-state bursts and indicate that neither enzyme utilizes a branched kinetic pathway for the hydrolysis of nitrocefin. Rapid-scan UV−vis studies revealed the presence of a short-lived intermediate whose concentration and lifetime were dependent upon the concentration of enzyme and nitrocefin. The structure of this intermediate could possibly serve as a

guide for the design and preparation of a specific inhibitor of metallo-β-lactamases. Attempts to trap this intermediate and to spectroscopically characterize it are currently in progress.

ACKNOWLEDGMENT

We thank Professor Gilbert Gordon at Miami University for the use of his rapid scan/stopped-flow UV−vis spectrophotometer, Abraham Sissoko for helpful discussions regarding the operation of the instrument, and Dr. Zhigang Wang of Penn State University for helpful discussions regarding analysis of the data and for sharing results on CcrA before publication. We thank Professor Carl Frieden for his assistance in the use of the new versions of KINSIM and FITSIM, Smith-Kline Beecham for providing a sample of BRL42715, and Drs. Steven Gamblin and James Spencer for sharing information about the crystal structure of L1 before publication.

REFERENCES

1. Knowles, J. R. (1985) *Acc. Chem. Res. 18*, 97−104.
2. Richmond, M. H., and Sykes, R. B. (1973) *Adv. Microb. Physiol. 9*, 31−88.
3. Ambler, R. P. (1980) *Philos. Trans. R. Soc. London B 289*, 321−331.
4. Bush, K. (1989) *Antimicrob. Agents Chemother. 33* (3), 259−263.
5. Bush, K. (1989) *Antimicrob. Agents Chemother. 33* (3), 264−270.
6. Bush, K. (1989) *Antimicrob. Agents Chemother. 33* (3), 271−276.
7. Bush, K., Jacoby, G. A., and Medeiros, A. A. (1995) *Antimicrob. Agents Chemother. 39* (6), 1211−1233.
8. Payne, D. J. (1993) *J. Med. Microbiol. 39*, 93−99.
9. Valladares, M. H., Felici, A., Weber, G., Adolph, H. W., Zeppezauer, M., Rossolini, G. M., Amicosante, G., Frere, J. M., and Galleni, M. (1997) *Biochemistry 36*, 11534−11541.
10. Rossolini, G. M., Franceschini, N., Riccio, M. L., Mercuri, P. S., Perilli, M., Galleni, M., Frere, J. M., and Amicosante, G. (1998) *Biochem. J. 332*, 145−152.
11. Ullah, J. H., Walsh, T. R., Taylor, I. A., Emery, D. C., Verma, C. S., Gamblin, S. J., and Spenser, J. (1998) *J. Mol. Biol. 284*, 125−136.
12. Carfi, A., Pares, S., Duee, E., Galleni, M., Duez, C., Frere, J. M., and Dideberg, O. (1995) *EMBO J. 14* (20), 4914−4921.
13. Concha, N. O., Rasmussen, B. A., Bush, K., and Herzberg, O. (1996) *Structure 4*, 823−836.
14. Crowder, M. W., Wang, Z., Franklin, S. L., Zovinka, E. P., and Benkovic, S. J. (1996) *Biochemistry 35*, 12126−12132.
15. Crowder, M. W., Walsh, T. R., Banovic, L., Pettit, M., and Spencer, J. (1998) *Antimicrob. Agents Chemother. 42* (4), 921−926.
16. Orellano, E. G., Girardini, J. E., Cricco, J. A., Ceccarelli, E. A., and Vila, A. J. (1998) *Biochemistry 37*, 10173−10180.
17. Payne, D. J., Bateson, J. H., Gasson, B. C., Proctor, D., Khushi, T., Farmer, T. H., Tolson, D. A., Bell, D., Skett, P. W., Marshall, A. C., Reid, R., Ghosez, L., Combret, Y., and Marchand-Brynaert, J. (1997) *Antimicrob. Agents Chemother. 41* (1), 135−140.
18. Payne, D. J., Bateson, J. H., Gasson, B. C., Khushi, T., Proctor, D., Pearson, S. C., and Reid, R. (1997) *FEMS Microbiol. Lett. 157*, 171−175.
19. Saino, Y., Kobayashi, F., Inoue, M., and Mitsuhashi, S. (1982) *Antimicrob. Agents Chemother. 22* (4), 564−570.
20. Paton, R., Miles, R. S., and Amyes, S. G. B. (1994) *Antimicrob. Agents Chemother. 38* (9), 2143−2149.
21. Wang, Z., and Benkovic, S. J. (1998) *J. Biol. Chem. 273* (35), 22402−22408.
22. Walsh, T. R., Hall, L., Assinder, S. J., Nichols, W. W., Cartwright, S. J., MacGowan, A. P., and Bennett, P. M. (1994) *Biochim. Biophys. Acta 1218*, 199−201.
23. Denton, M. (1997) *Rev. Med. Microbiol. 8*, 15−19.
24. Benson, K. K., Raddatz, J. K., and Rotschafer, J. C. (1996) *J. Infect. Dis. Pharmacother. 2*, 1−14.
25. Cullmann, W. (1991) *Chemotherapy 37*, 246−259.
26. Onate, J., Aquirrebengoa, K., Ibanez de Maeztu, J. C., Hernandez, J. L., and Montejo, M. (1995) *Enferm. Infec. Microbiol. Clin. 13* (3), 188−190.
27. Muder, R. R., Yu, V. L., Dummer, J. S., Vinson, C., and Lumish, R. M. (1987) *Arch. Int. Med. 147*, 1672−1674.
28. Spencer, R. C. (1995) *J. Hosp. Infect. 30*, 453−464.
29. Khardori, N., Elting, L., Wong, E., Schable, B., and Bodey, G. P. (1990) *Rev. Infect. Dis. 12* (6), 997−1003.
30. Soriano, V., Valencia, E., Alba, A., and Gonzalez-Lahoz, J. (1994) *Med. Clin. 102* (10), 399.
31. Poulos, C. D., Matsumura, S. O., Willey, B. M., Low, D. E., and McGeer, A. (1995) *Antimicrob. Agents Chemother. 39* (10), 2220−2223.
32. Mett, H., Rosta, S., Schacher, B., and Frei, R. (1988) *Rev. Infect. Dis. 10* (4), 765−819.
33. Walsh, T. R., Payne, D. J., Neville, T., Tolson, D., MacGowan, A. P., and Bennett, P. M. (1997) *Antimicrob. Agents Chemother. 41*, 1460−1462.
34. Farmer, T. H., Page, J. W. J., Payne, D. J., and Knowles, D. J. C. (1994) *Biochem. J. 303*, 825−830.
35. Crowder, M. W., Stewart, J. D., Roberts, V. A., Bender, C. J., Tevelrach, E., Peisach, J., Getzoff, E. D., Gaffney, B. J., and Benkovic, S. J. (1995) *J. Am. Chem. Soc. 117*, 5627−5634.
36. Stewart, J. D., Roberts, V. A., Crowder, M. W., Getzoff, E. D., and Benkovic, S. J. (1994) *J. Am. Chem. Soc. 116*, 415−416.
37. Fierke, C. A., Johnson, K. A., and Benkovic, S. J. (1987) *Biochemistry 26* (13), 4085−4082.
38. Barshop, B. A., Wrenn, R. F., and Frieden, C. (1983) *Anal. Biochem. 130*, 134−145.
39. Dang, Q., and Frieden, C. (1997) *Trends Biochem. Sci. 22*, 317.
40. Frieden, C. (1993) *Trends Biochem. Sci. 18*, 58−60.
41. Frieden, C. (1994) *Trends Biochem. Sci. 19*, 181−182.
42. Bruist, M. F. (1998) *J. Chem. Educ. 75* (3), 372−375.
43. O'Callaghan, C. H., Morris, A., Kirby, S. M., and Shingler, A. H. (1972) *Antimicrob. Agents Chemother. 1* (4), 283−288.
44. Fersht, A. (1985) *Enzyme Structure and Mechanism*, 2nd ed., W. H. Freeman and Co., New York.
45. Matagne, A., Ledent, P., Monnaie, D., Felici, A., Jamin, M., Raquet, X., Galleni, M., Klein, D., Francois, I., and Frere, J. M. (1995) *Antimicrob. Agents Chemother. 39* (1), 227−231.
46. Sutton, B. J., Artymiuk, P. J., Cordero-Borboa, A. E., Little, C., Phillips, D. C., and Waley, S. G. (1987) *Biochem. J. 248*, 181−188.
47. Fitzgerald, P. M. D., Wu, J. K., and Toney, J. H. (1998) *Biochemistry 37*, 6791−6800.
48. Concha, N. O., Rasmussen, B. A., Bush, K., and Herzberg, O. (1997) *Protein Sci. 6*, 2671−2676.
49. Bounaga, S., Laws, A. P., Galleni, M., and Page, M. I. (1998) *Biochem. J. 331*, 703−711.
50. Wang, Z., Fast, W., and Benkovic, S. J. (1998) *J. Am. Chem. Soc. 120*, 10788−10789.
51. Bicknell, R., and Waley, S. G. (1985) *Biochemistry 24*, 6876−6887.
52. Bicknell, R., Schaffer, A., Waley, S. G., and Auld, D. S. (1986) *Biochemistry 25*, 7208−7215.

BI9826512